Ad Hoc Networks 86 (2019) 166–178

Contents lists available at ScienceDirect

Ad Hoc Networks

journal homepage: www.elsevier.com/locate/adhoc

A new CubeSat design with reconfigurable multi-band radios for dynamic spectrum satellite communication networks

Ian F. Akyildiz [a,*], Josep M. Jornet [b], Shuai Nie [a]

[a] Broadband Wireless Networking Laboratory, School of Electrical and Computer Engineering, Georgia Institute of Technology, Atlanta, GA 30332, United States

[b] Department of Electrical Engineering, University at Buffalo, The State University of New York, Buffalo, NY 14260, United States

ARTICLE INFO

Article history:
Available online 6 December 2018

Keywords:
CubeSats
Small satellites
Satellite networks
Multi-band radios
Terahertz communication
Dynamic spectrum
5G and beyond

ABSTRACT

Small satellites, or CubeSats, are envisioned as a promising solution for future satellite communication networks because of their low costs and short deployment cycle. Currently, CubeSats communicate at conventionally allocated satellite communication frequencies. However, with the increase in the number of CubeSats, CubeSat-enabled communication systems, and many new use cases, new spectrum bands and a more efficient spectrum usage are needed. In this paper, a novel CubeSat design with reconfigurable multi-band radios for communication in dynamic frequencies is proposed.The multi-band radio design is realized by two complementary approaches, namely, an electronics-based and a photonics-based approach. The multi-band communication covers a wide range from radio frequencies (2–30 GHz), millimeter wave (30–300 GHz), Terahertz band (up to 10 THz), and optical frequencies (with typical bands of 850 nm/350 THz, 1300 nm/230 THz, and 1550 nm/193 THz). A thorough link budget analysis is conducted to demonstrate the potential of the proposed multi-band architecture for space information networks. Key parameters in the satellite constellation design are investigated to explore the feasibility of deployment at different altitudes in the exosphere orbit (500 km and above). A continuous global coverage is demonstrated to serve the *Internet of Space Things*, a new paradigm for next generation satellite communication networks.

1. Introduction

The commercial use of space requires the development of reliable and economic solutions to serve various applications including sensing, imaging, navigation and communication, among others. Such services are currently supported by traditional satellites in Low Earth Orbits (LEO), Medium Earth Orbits (MEO) and Geosynchronous Equatorial Orbits (GEO). Nevertheless, existing satellites have several major drawbacks. First, the very high costs associated with the design, construction, launch and operation of traditional satellites and satellite networks result in a very high entry barrier for new operators and vendors. For example, the cost of developing and deploying the Iridium Next system is expected to exceed $3 billion [1]. Consequently, the use of satellites has been restricted to a few major players. In addition, traditional satellites have very long development cycles, which can range from three years for commercial ventures to ten or more years for government initiatives [2]. Moreover, traditional satellite programs do not make use of sequential redundancy [3], i.e., a new development program is usually started only after the previous program has been fully deployed, making it difficult to adapt to the rapidly changing market needs.

Recognizing those deficiencies, the satellite landscape has witnessed the emergence of a new class of miniaturized satellites known as CubeSats. Originally envisioned for university education and research purposes, CubeSats are seen as a promising solution to realize global satellite networks at much lower costs [4]. In addition, the short timeframe from development to operation makes CubeSats an efficient deployment option, very different from traditional satellite networks. CubeSats have uniform cubic sizes of payload systems denoted as 1U, 2U, etc., where “U” means a $10 \times 10 \times 10\,\text{cm}^3$ cube, and can be used for applications in numerous research fields including biochemistry, astrophysics, and telecommunications [5].

Recently, many commercial solution providers have targeted CubeSats to serve in LEO to provide services including Earth remote sensing, weather forecasting, and machine to machine communication, as shown in Table 1. For instance, Planet Labs has re-

* Corresponding author.
E-mail addresses: ian@ece.gatech.edu (I.F. Akyildiz), jmjornet@buffalo.edu (J.M. Jornet), shuainie@ece.gatech.edu (S. Nie).

https://doi.org/10.1016/j.adhoc.2018.12.004
1570-8705/

Table 1
Existing or Planned CubeSats-based Satellite Services [6–13].

Name of CubeSat	Iridium NEXT SensorPoD	Dove	MarCO	Astrocast	Fleet	KIPP	AISTECHSAT
Company/Agency, Country	Iridium Communications, US	Planet Labs, US	NASA, US	ELSE, Switzerland	Fleet, Australia	Kepler, Canada	Aistech, Spain
Purpose	Sensing and communication	Earth imaging	Mars exploration	IoT and M2M	IoT	Satellite backhaul	IoT, M2M, asset tracking
ISL Capability	Only to the host Iridium NEXT satellites	No	No	Yes	n/a	n/a	n/a
Year of First Launch	2015	2015	2018	2018	2018	2018	2018
Orbit Altitude	780 km	420 and 475 km	n/a	n/a	580 km	n/a	n/a
Number of CubeSats in Constellation	66	175	2	64	100	140	100
Form Factor	4.5U	3U	6U	n/a	3U + 12U	3U	6U
Weight	4–5 kg	5.8 kg	14 kg	n/a	n/a	n/a	n/a
Frequency	Ku-band	X-band	X-band	L-band	n/a	Ku-band	n/a
Self-sustained	No	Yes	Yes	Yes	Yes	Yes	Yes

Note: "n/a" means the parameter is not available in published sources.

cently launched a total of 175 CubeSats named "Doves" to support high-resolution Earth imaging services [8]. CubeSats are also deployed in deep space for missions including interplanetary data relaying, sensing and monitoring on the Moon, Mars, and several asteroids, as well as even further in deep space. For example, the Mars Cube One (MarCO) mission from NASA consists of a pair of CubeSats aimed at the exploration of Mars. The pair, MarCO-A and MarCO-B, was successfully launched in May 2018 and planned to fly by Mars in November 2018 [9]. Even more promising CubeSat missions will be enabled with future advancements in physics, electronics, and telecommunications.

With the proliferation of CubeSat-enabled applications and, consequently, the increase in the number CubeSats in different orbits, there has been an exponential increase in the use of the space communication frequency spectrum [14]. Communication between satellites is needed both to enable the exchange of control and data information between CubeSats as well as to realize a globally connected network with ground infrastructure. Currently, conventional satellite networks as well as recently-deployed CubeSat networks rely on the use of specific frequency sub-bands within the authorized spectrums regulated by the Federal Communications Commission (FCC) under 47 CFR 97.207 and regulatory framework of the International Telecommunications Union (ITU). Traditionally, the use of higher frequency bands has been discouraged due to their much higher path loss and, thus, shorter transmission distance between satellites, which would have required the deployment of denser satellite constellations. Nevertheless, the much lower cost and development timeline of CubeSats open the door to considering higher frequency bands for communication, including the millimeter wave (mm-wave) (30–300 GHz) and the Terahertz (THz) bands (0.1–10 THz) as well as the infra-red and visible spectral bands (200–400 THz). Ultimately, efficient techniques for spectrum access, management, and sharing are needed to support the next generation satellite services.

In this paper, we propose a CubeSat design able to support multi-band wireless communication at microwaves, mm-wave, THz-band and optical frequencies. Multi-band communication is needed for CubeSats to meet the throughput requirements for inter-satellite and ground-to-satellite data-intensive applications. In our proposed architecture, CubeSats with an altitude between 500 and 900 km above the Earth can transmit, receive, and store data with high throughput in a global coverage constellation. This architecture can significantly leverage the capabilities of current CubeSat networks, and will be fundamental for future interplanetary CubeSat networks. We envision that the CubeSat networks will conceive the "*Internet of Space Things* (IoST)", a paradigm-shift architecture to leverage the cyber-physical system with another degree of freedom in the space for global process control and optimization. The detailed network architecture of the IoST is elaborated in [6].

The novelties of our architecture are:

1. Multi-band radios covering wide spectrums at microwaves, mm-wave, THz band, and optical frequencies to accommodate high-throughput services. The key enabling device technologies include (i) hybrid integration of two complementary signal generation, modulation, detection and demodulation approaches, namely, an electronics-based approach and a photonics-based approach, and (ii) enhancement and exploitation of the intermediate products and harmonics generated in the process of frequency up and down conversion;
2. Foldable multi-band antenna arrays based on new materials such as graphene, which allow the creation of programmable antenna architectures with tunable frequency and radiation diagram. The frequency and space beamforming capabilities of such arrays are dynamically exploited to accommodate different communication requirements;
3. Deep neural networks-enabled resource allocation strategies for self-learning and optimization of CubeSat networks to adaptively determine the optimal combination of specific frequency channel, transmit power, antenna gain, modulation and coding scheme.

The remainder of the paper is organized as follows. After introducing the existing CubeSat architecture in Section 2, in Section 3, we describe the multi-band communication technology for the next generation CubeSats, including innovative transceivers and antennas. Then, we describe the communication aspects between CubeSats as well as between CubeSats and ground devices, including types of links, physical and link layers solutions, and open research challenges, in Section 4. Key deployment aspects, including CubeSat constellation planning in light of both sensing coverage and satellite connectivity, are studied in Section 5, and, finally, we conclude the paper in Section 6.

2. Current CubeSat architecture

The design of a CubeSat follows standards based on the research collaborations among universities and research labs, which guarantees the unification among payloads and launchers and optimize the capabilities of miniaturized payloads [15]. According to the specifications set by NASA, CubeSats cannot contain any propulsion systems, hence they can only be deployed to the target orbit as secondary payloads via an airborne launch system in a

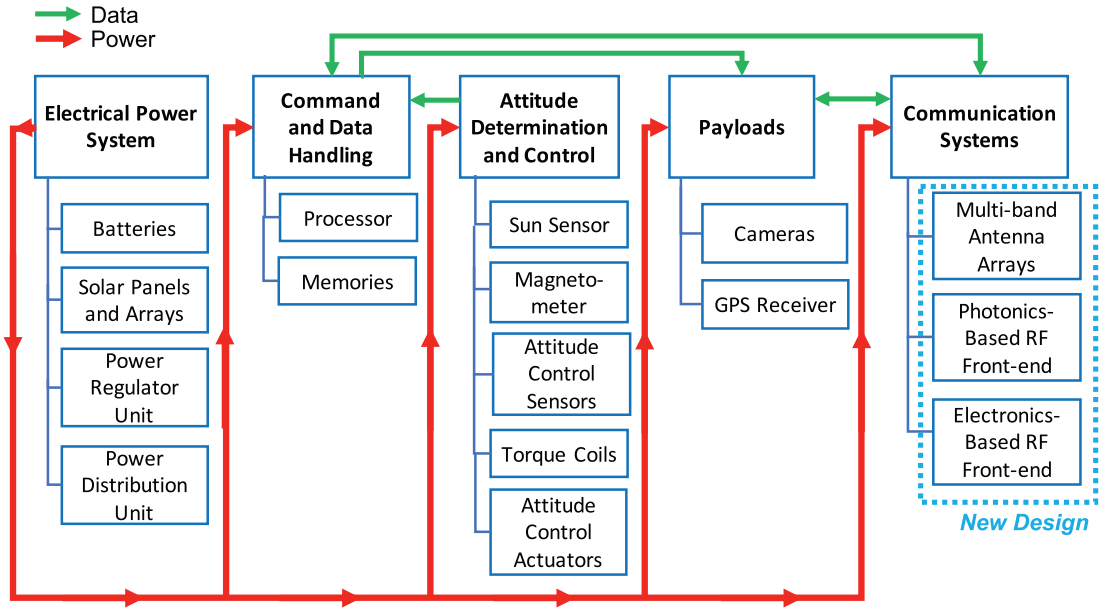

Fig. 1. Basic functional components of next-generation CubeSats.

rocket (e.g., Space-X) or from the International Space Station (ISS) [16]. In both cases, the deployment stage is carried out through a poly-picosatellite orbital deployer (P-POD) system [17], which currently supports CubeSats of size up to 3U. In the next sections, we describe the main components in current CubeSat architectures, which are summarized in Fig. 1.

2.1. Electrical Power System (EPS)

The EPS serves as the energy source to perform all necessary sensing, processing, and communication tasks. It includes subsystems to perform energy conversion, power regulation and control, energy storage, and distribution [18]. The major energy source is the Sun and, thus, solar panels and high-capacity batteries are utilized to provide highest efficiency even when the CubeSat is not covered by sunlight. The EPS includes the follow components:

- *Batteries*: The batteries in existing CubeSats commonly use lithium polymer cells with a nominal voltage level of 5 V with high energy densities and a robust protection architecture according to the standard. The batteries also provide extra protection against overcharge, over-discharge, over-current, over-voltage, and over-temperature.
- *Solar panels and arrays*: State-of-the-art solar panels generally consists of III-V semiconductor-based solar cells (e.g., GaAs) triple junction solar cells), temperature sensors and Sun sensors. Before the on-orbit deployment, the solar panels are folded inside the launch vehicle. Once in orbit, the solar panels are expanded to conduct energy harvesting, temperature sensing, and other tasks.

2.2. Command and Data Handling (C&DH)

The purpose of the C&DH board is to command the subsystems of CubeSats. The subsystems include performing Earth imaging operations, commanding radio to beacon, transmitting data, receiving commands and data, changing configurations, and commanding EPS to power on or off. The C&DH consists of two processing units. The processing core of the C&DH interprets control commands and schedules actions, whereas small form-factor, low power-consumption micro-controllers are responsible for communicating with the CubeSat's other subsystems.

2.3. Attitude Determination and Control System (ADCS)

Another crucial system inside a CubeSat is the ADCS, which guarantees the stability of payloads, manages the position and pointing accuracy of antennas, and assists optical control to provide fine pointing. It contains several sensors, actuators, and magnetometers to measure the magnetic field near orbit [19].

2.4. Payloads

There is a plethora of payloads that a CubeSat can incorporate. The most advanced systems include multi-frequency (infrared, visible, ultra-violet) orthophoto cameras which are capable of capturing imagery at a resolution of 10–15-m ground sample distance, telescopes that can observe from surrounding satellites to deep space objects, and a series of sensors for space environment monitoring such as temperature and gas concentration among others. The image sensing capability equipped on CubeSats can reach a radiometric resolution of 16 bits with a spatial granularity or positional accuracy of less than 10 m root mean square error.

2.5. Communication system

Currently, CubeSats have limited communication capabilities to ground infrastructure. The available frequency bands for communication are the S-band (2–4 GHz), C-band (4–8 GHz), X-band (8–12 GHz), Ku-band (12–18 GHz), and Ka-band (26.5–40 GHz). These frequency bands are also being heavily utilized by other satellite communication and links between space shuttles and the ISS, as well as terrestrial wireless networks including IEEE 802.11 series, which can cause severe interference and thus degrade system performance. In the next section, we present the new communication architecture for our CubeSat design.

3. Our new hardware design for next generation CubeSats

Our new hardware design of next-generation CubeSats incorporates innovative multi-frequency transceivers and antenna arrays needed to support high-throughput inter-satellite and ground-satellite links needed in CubeSat-enabled satellite applications. In

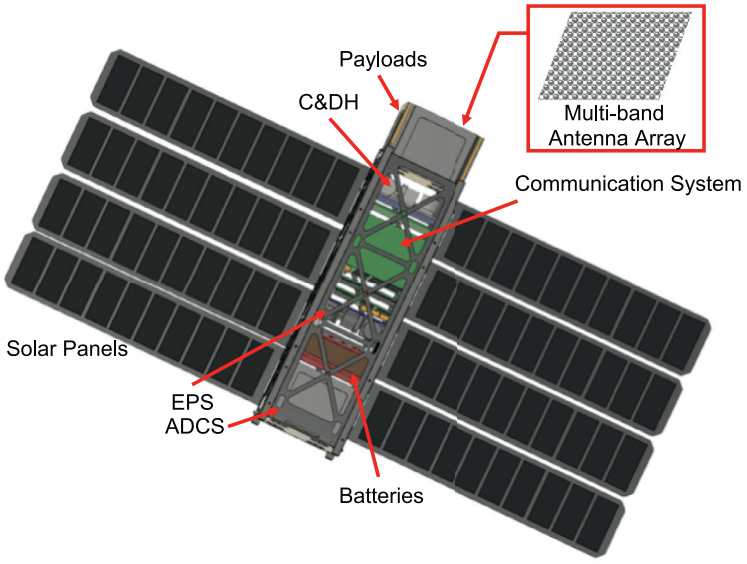

Fig. 2. Preliminary design of a next-generation 3U CubeSat with solar panels expanded and basic functional components indicated by arrows.

order to meet the requirements of future CubeSat use cases and accommodate necessary subsystems and payloads, we propose new CubeSat with the dimension of 3U ($10\,\text{cm} \times 10\,\text{cm} \times 34\,\text{cm}$) and a maximum weight of 5 kg, as illustrated in Fig. 2. This new design allows the antenna arrays to be stowed during launch and pre-deployment. The details of the proposed multi-frequency transceivers and antenna arrays are described in Sections 3.1 and 3.2, respectively.

3.1. Multi-frequency transceiver design from RF to THz bands to optical frequencies

To overcome the spectrum scarcity and capacity limitations in current satellite networks, we propose the utilization of multiple frequency bands, from RF to THz, and to optical frequencies, for next-generation CubeSat communication systems. For this, frequency-agile ultra-broadband reconfigurable systems able to communicate over the broad electromagnetic (EM) spectrum ranging from hundreds of MHz up to optical frequencies need to be developed. Between the two ends of the spectrum, the mm-wave and, especially, the THz-band frequencies provide new opportunities for high-speed wireless communications. Due to recent major progress in device development at these frequencies [20,21], it is possible to enable communication at such high frequency bands. While molecular absorption by oxygen and water vapor at mm-wave and THz-band cause heavy attenuation to signals on the ground, such effect does not exist in space because of the very low concentration of absorbing molecules above the atmosphere.

Millimeter-wave and THz-band communication exhibit several key advantages over RF communications:

- Thanks to the very large available bandwidth at mm-wave and THz frequencies, even very simple modulation and coding strategies can support from the start much higher bit-rates than existing RF systems.
- Thanks to the small wavelength at mm-wave and THz frequencies, the size of antenna arrays can be significantly reduced. More antenna elements can fit per unit area of the array, enabling new massive and ultra-massive MIMO communication schemes.
- Thanks to the directional propagation of mm-wave and THz frequency waves, interference between satellites is potentially much lower than at RF frequencies.

It must be noted that the use of optical communications for satellite networks has also been proposed [22,23]. Compared to optical frequencies, the mm-wave and, specially, the THz-band supports similarly large transmission bandwidths, which are mainly limited not by the physics of the channel, but by the speed of the electronic and opto-electronic components. Moreover, the much narrower transmission beams in optical systems further increases the alignment requirements between the transmitting and receiving satellite. In light of these observations, the THz band (0.1–10 THz) seems to offer a compromise between RF (2–300 GHz) and optical bands (with typical bands of 850 nm/350 THz, 1300 nm/230 THz, and 1550 nm/193 THz). In any case, ultimately, the synergistic use of the spectrum if needed.

To enable the proposed multi-frequency communication system, new transceiver architectures are needed. Three metrics weigh in the design of a reliable and efficient transceiver suitable to generate signals at various frequency bands for space communication and networking, namely, (i) dimension constraints, (ii) power source and energy consumption, and (iii) achievable performance. In particular, the dimension of the transceiver has to follow the standard specified in CubeSat architecture. Besides the aforementioned benefits of operating at mm-wave and THz-band frequencies, one additional advantage of operating in space is the fact that devices can be naturally operating at a low temperature, without the need of cooling components or cryostats. This can further lead to compact communication systems for CubeSats.

We propose two parallel approaches to realize the proposed multi-band transceivers, namely, multi-stream electronic up-converting chains and optical down-converting chains.

3.1.1. Multi-stream electronic frequency up-converting chains

While direct-generation mm-wave and THz sources have been envisioned [24,25], currently, the most common option to generate mm-wave and THz signals is through frequency multiplication and up-conversion [26,27]. Conventionally, only the final up-converted signals are used as the output and the intermediate products are discarded. However, by taking advantage of these intermediate frequencies, we can leverage the up-conversion chain to generate multi-streams of signals to be fully utilized as carriers in the multi-band communication system. As illustrated in Fig. 3, the general idea is to use frequency splitters after frequency multipliers in order to extract the intermediate frequencies for outputs. The signal

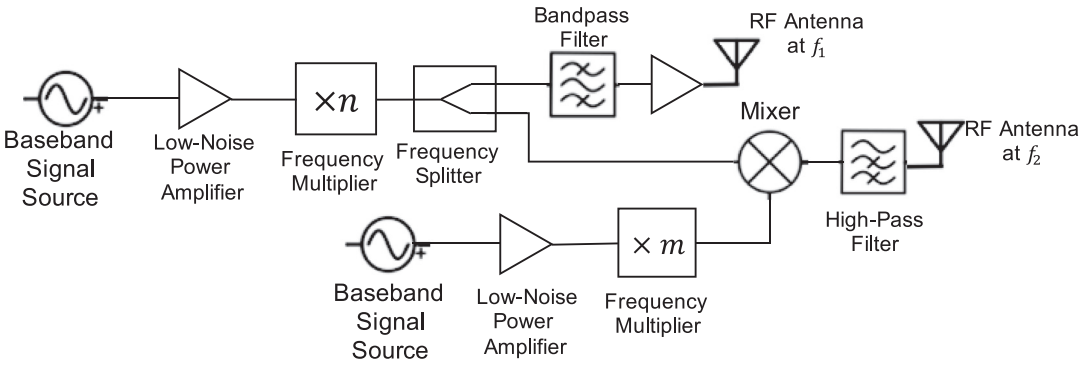

Fig. 3. A block diagram of all-spectrum signal front-end by the electronics-based approach.

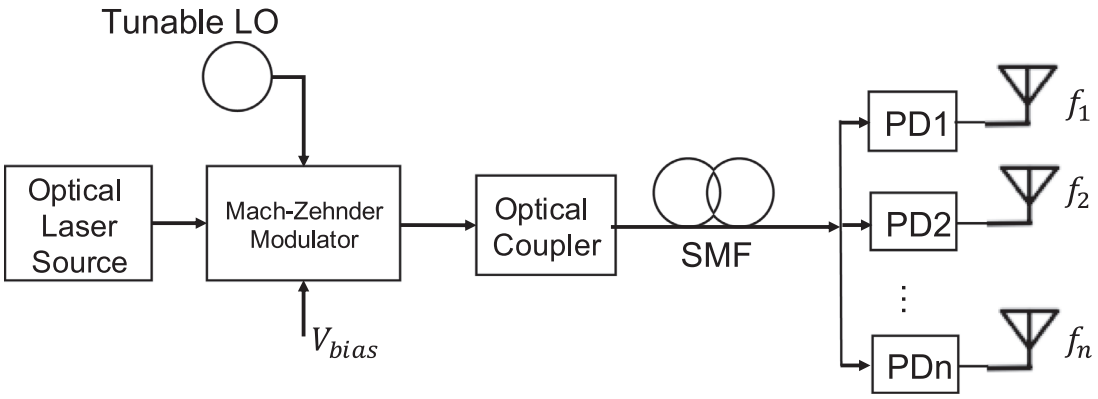

Fig. 4. A block diagram of multi-frequency band front-end by the photonics-based approach.

at frequency f_1 is considered as the intermediate output when producing signals at a higher frequency f_2. Similar structures can be cascaded to provide more output streams.

The main components of the electronic transceiver include *frequency multipliers, mixers, splitters, amplifiers, and filters*. The function of frequency multipliers, which are usually implemented as chains of frequency doublers or triplers, is to increase the frequency of the local oscillator (LO) to the desired radio frequency or to an intermediate frequency (IF). Mixers combine two input signals to generate the output at the sum of their frequencies. Frequency splitters divide the input signal into two identical output signals for further processing. Amplifiers enhance the amplitude of the input signal, while filters, including bandpass and high-pass filters, can eliminate unwanted harmonics to improve the spectrum efficiency. The proposed structure leverages the state of the art in RF, mm-wave and THz transceivers, and can only benefit from further developments.

3.1.2. Photonics frequency down-conversion chains

Besides RF up-conversion to mm-wave/THz bands, there is also an alternative approach to generate multi-frequency by down-converting optical signals which can fit in the limited space in IoST CubeSats while providing satisfying multi-band signal generation. These recent research advances are enabled by photonics-based RF signal generation based on a silicon photonics chip [28–30]. The major components of the photonics-based approach include *a laser signal source and a Mach–Zehnder modulator*. With similar ideas of taking advantage of the multi-stream signals as in Section 3.1.1, as shown in Fig. 4, multi-band signals can be generated by the approach of heterodyning two input signals with a Mach–Zehnder modulator, thus producing an RF signal with a frequency equal to the difference between the two inputs as the final output, while maintaining the two input signals also as two output streams. With a tunable LO, multi-frequency band signals can be generated as the output [31]. Additionally, the stability of the photonics-based RF signals is directly dependent on the stability of the laser sources. Therefore, in the CubeSat design, mode-locked lasers are preferred to generate stable signal source [32]. Then a single-mode optical fiber is used to deliver the down-converted signal to the antenna side.

3.2. Multi-frequency antenna systems

In addition to the transceivers, multi-frequency antenna systems as well as very high gain directional antennas are needed to combat the very long transmission distances. While fixed directional antennas, such as horn antennas, mounted on mechanical steering systems, could be utilized, electronically-controlled phased antenna arrays are preferred due to their much higher flexibility. When moving to higher frequency bands, antennas become smaller and, thus, much denser antenna arrays can be built. As we will discuss in Section 4, these very large antenna arrays are at basis of massive and ultra-massive MIMO communication schemes.

In order to create a multi-band antenna array, different technologies can be leveraged. On the one hand, *physically reconfigurable antennas* based on nano- or micro-electromechanical (NEMS/MEMS) or origami structures have been proposed as a way physically change the size of the radiating elements and, thus, their resonant frequency [33,34]. The main challenges with this approach are the delay associated to the control of the NEMS/MEMS systems, specially when targeting very high data-rates, as well as the size and integration complexity of NEMS for the THz-band antennas. On the other hand, new materials such as graphene can be leveraged to create *software-defined or electronically tunable*

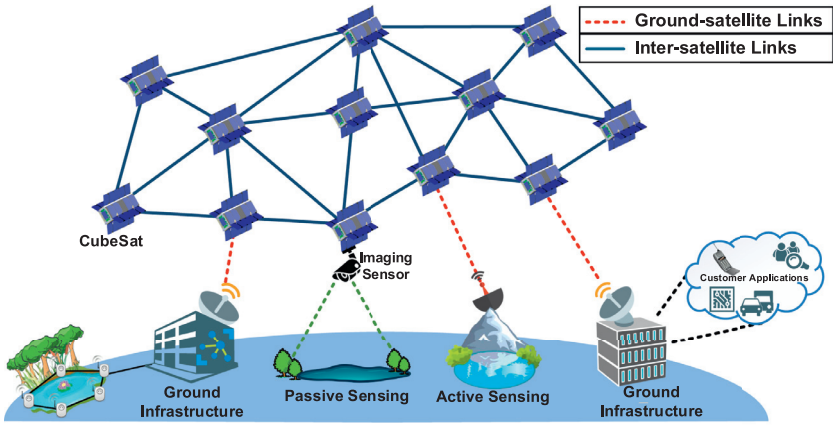

Fig. 5. Overview of CubeSat links. The ISLs relay data packets and control signals among CubeSats, while the GSLs connect the ground infrastructure and CubeSats to perform sensing and data relay tasks.

nano-antennas and nano-antenna arrays [35,36]. Indeed, the resonant frequency of graphene-based plasmonic nano-antennas can be controlled by modulating the graphene Fermi energy or chemical potential. As a result, without physically changing the antenna size, one antenna can be tune to resonate at different bands. While graphene can be utilized for THz frequencies, other nanomaterials and metamaterials are needed to achieve a similar behavior at lower bands.

Besides transmit antenna arrays, reflector antenna arrays can be utilized to fit the multi-frequency CubeSat links. *Reflectarray antennas* have been widely utilized in radars, point-to-point links, and satellite communications because of their flexibility and low cost [37]. Based on principles of phased arrays and geometrical optics, electronically tunable reflector antenna arrays can realize dynamically adjustable radiation patterns. Specifically, the phase shift of each element in the array can be controlled electronically and will jointly form an array pattern to receive or transmit the signal to or from desired directions. Compared to traditional phased arrays that require complicated phase shifter circuits and suffer from high transmission line loss at higher frequencies, reflector antenna arrays are simpler in mass production and have higher energy efficiency because there is no need for transmission lines, which make them suitable to be attached to CubeSats with limited dimensions. Moreover, we leverage the conventional design of reflectarrays to a series of foldable multi-band antenna arrays which can be attached to the body of CubeSats and expanded to larger sizes to achieve high gain, enhanced directivity, and high efficacy in multi-band operation. The operation of folding and expansion can be controlled adaptively given the requirements of communication tasks.

3.3. Hardware development and integration

We are currently working towards the development and integration of the multi-band front-ends, with a focus on the electronics approach. Many of the main components, including compact synthesizers for the LO at tens of GHz as well as frequency multipliers (doublers, triplers), power amplifiers, mixers and power dividers are commercially available for mm-wave frequencies. When moving towards the frequency multipliers for higher frequencies, currently, the technology able to generate the highest power is the Gallium Nitride (GaN) Schottky-diode-based technology developed by the NASA Jet Propulsion Laboratory [38]. Using this technology, integrated systems at different frequencies ranging from 180 GHz to 1.6 THz, with output power ranging from 500 to 0.7 mW, respectively, have been demonstrated. Some of these devices are available to the team through a collaboration agreement.

For the generation of the different control signals as well as data signal processing, high-performance FPGAs are needed. Currently, we are leveraging the software-defined-radio (SDR) platform developed by National Instruments, which is able to support real-time bandwidths of 2 GHz [39]. Each NI baseband processor consists of several high-performance Xilinx Virtex 7 FPGAs. The number of FPGAs will ultimately depend on the control and signal processing requirements as well as on the power and energy consumption of the communication unit of the CubeSat, which we are currently developing.

4. Multi-band CubeSat communications

The multi-frequency transceivers and antenna arrays architectures introduced in the previous section will enable innovative, faster, and more spectrum-efficient satellite communication systems. In this section, we conduct a link budget analysis and discuss the communication aspects at the physical and link layers of next generation CubeSat-enabled networks.

4.1. Types of CubeSat links

There are two types of links in satellite communications, namely, inter-satellite links (ISLs) and ground-to-satellite links (GSLs), as shown in Fig. 5. The ISLs include data relay and control links among CubeSats, while the GSLs consist of duplex links between CubeSats and ground infrastructure.

4.1.1. Inter-satellite links

Communication between CubeSats in orbit are enabled by ISLs, also known as “crosslinks”. Analogous to terrestrial Internet backbone links, ISLs require very high capacity in order to be able to handle the aggregate data flows from ground devices as well as satellite data and, ultimately, reduce the total transmission time significantly. For this, we propose to utilize multiple mm-wave and THz bands at 0.06, 0.12, 0.18, 0.3, 0.6, and 1 THz for ISLs. As discussed in Section 3.1, the very low concentration of molecules in the exosphere eliminates the molecular absorption problem, which is one of the main bottlenecks for on-the-ground mm-wave and THz-band communications.

To assess the feasibility and derive the gain requirements for CubeSats in ISLs, we conduct a link budget analysis. The antenna system used in our simulation is the reconfigurable reflectarray antenna discussed in Section 3.2 and modeled using the Antenna Magus in the CST Studio Suite at the aforementioned frequencies.

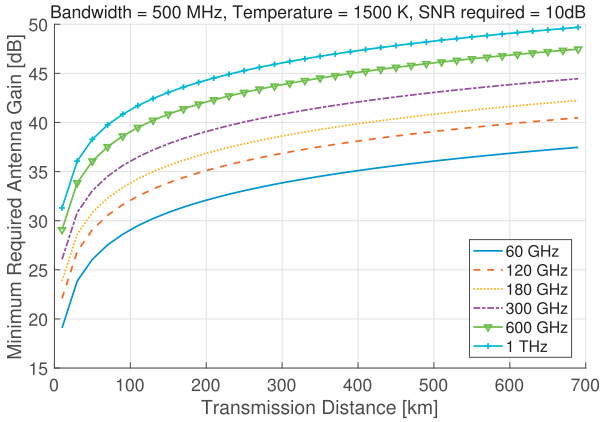

Fig. 6. Minimum required gain at the receiver in ISLs to maintain a 10 dB SNR at several typical communication frequencies in IoST.

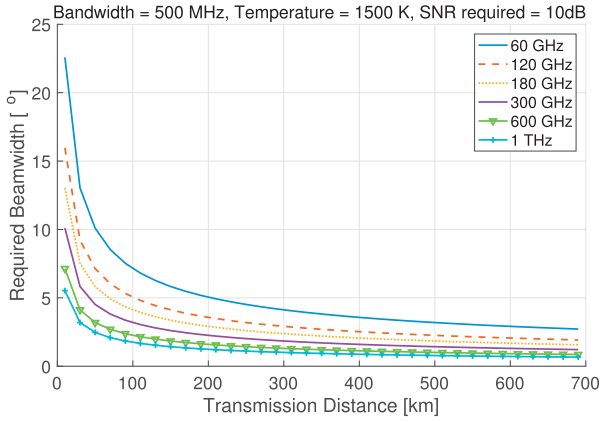

Fig. 7. Maximum allowable beamwidth at the receiver in ISLs to maintain a 10 dB SNR at several typical communication frequencies in IoST.

We consider that the minimum bandwidth for communication is 500 MHz and the maximum transmitted power is 10 W as specified in the CubeSat standard. In the exosphere, since the temperature is a function of altitude and can vary greatly from a few degrees above absolute zero to thousand degrees in Kelvin, the noise level can also vary gigantically, hence we study a typical value at 1500 Kelvin. In Figs. 6 and 7, we illustrate the minimum gain required and the maximum beamwidth allowable at the receiving CubeSat, respectively, to maintain a 10 dB Signal-to-Noise Ratio (SNR), for different frequency bands spanning from 60 GHz to 1 THz. From the simulation results, it is clear that higher gains are needed when increasing the transmission frequency, even in the absence of atmospheric losses. For the 500 MHz bandwidth, since the channel is symmetrical, the gain at each transceiver end is always under 50 dB, which can be achievable with the antenna technologies described in Section 3.2. Increasing the channel bandwidth by an order of magnitude would increase the required gain by 10 dB. In designing the CubeSat constellation, the distance between CubeSats not only influences the coverage of the Earth's surface, but also affects the achievable data rates. Hence in Section 5, we establish a two-step approach, in which we first discuss the minimum number of CubeSats to realize global coverage, then refine the design with the guarantee of reliable ISL throughput.

Due to the fact that distances between CubeSats in different orbital planes are constantly changing, the main problem for ISLs is the data exchange with CubeSats in motion. We envision a solution of data transmissions between two CubeSats in two phases, namely, the SDN-assisted transmission initialization and transmission process. In the initialization phase, the CubeSat which acts as a transmitter (Tx) will search for the CubeSat in next hop, with the help of a control framework, to relay data based on orbit data, energy capacity, operation status, and other factors. Then based on localized up-to-date information, the Tx will select the relay CubeSat which is idle, has enough energy capacity, and is orbiting towards the target terrestrial IoT network or CubeSat end-receiver (Rx). Once the initialization is completed, the frequency channel between the pair of Tx and relay CubeSats is fixed for transmission process. As long as the transceivers remain in line-of-sight (LoS), the signals can be transmitted continuously within a very short amount of time without any interference. This hop-by-hop approach is further complemented by the global network information available to the system control framework [6].

4.1.2. Ground-satellite links

Compared to ISL among CubeSats in the exosphere, where the atmospheric attenuation can be negligible and the received signal strength follows the Friis' law, the ground-to-satellite link is more challenging and complicated. The signals from CubeSats to ground stations will go through at least 500 km long distances traversing the dense atmosphere, which will greatly attenuate the signal strength. Some previous research focuses on the study of the ground-to-satellite link at mm-wave and THz band frequencies. The choice of ground station depends on the distribution of precipitable water vapor over the surface. It is shown that with optimal ground station locations, carrier bandwidths, and modulation schemes, the ground-to-satellite links at THz band can achieve 1 Tbps when fog, cloud, or air turbulence are absent [40]. The study also suggests to use airborne platform, such as small aircrafts or balloons, to forward signals from satellites to ground stations. However, deploying ground stations only at dry areas limits the potentials of ground-to-satellite link capacity. To solve this problem, at other locations where humidity is not suitable for THz link establishment, the lower bands can be used (e.g., the X-, Ku- and Ka- bands). These frequency bands can operate in environments where THz link might experience enormous atmospheric attenuation and molecular absorption.

In order to better utilize the available frequency resources and transmit the signals from CubeSats to ground stations, we propose *hybrid GSLs enabled by both microwave and mm-wave/THz bands.* The fundamental idea is to use a pilot signal at microwave frequencies to detect the viability of a ground-to-satellite link. If certain criteria are met for data transmission (i.e., CubeSat in line-of-sight (LOS) with ground station, weather permissible, and ground station idle), the data will be transmitted to ground station in Field-of-View (FOV) of the CubeSat with a dedicated channel and an ultra-low latency. We envision the wide spectrum ranging from 3 to 300 GHz can be utilized in GSL, because of the relatively smaller atmospheric and molecular attenuation rate compared to THz frequency bands through the Earth atmosphere. An exception occurs at 180 GHz with a noticeable drop in maximum achievable data rate is caused by the molecular absorption with a water vapor density of 7.5 g/m^3. For most frequency bands studied, in an environment with dry air and ambient temperature at 300 Kelvin (25°C), a data rate of 150 Gbps can be achieved at 300 GHz, as shown in Fig. 8. Even with a water vapor density of 7.5 g/m^3, the achievable data rates are on the Gbps-level.

4.2. Physical layer design

4.2.1. Massive and ultra-massive multiple-input multiple-output communications

In order to overcome the very high path loss in both ISLs and GSLs, very high gain directional antenna systems are required.

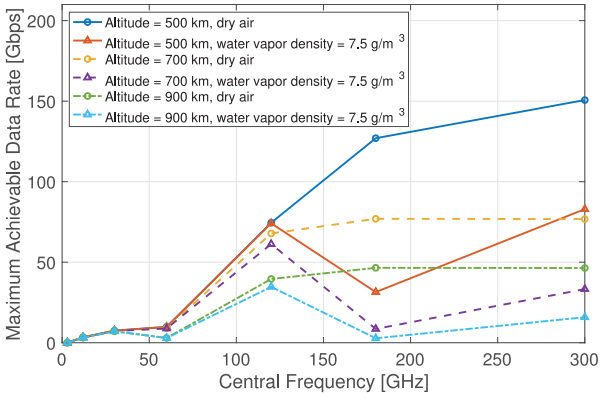

Fig. 8. Achievable data rates in GSL at several communication frequencies in both dry air and with water vapor density of 7.5.

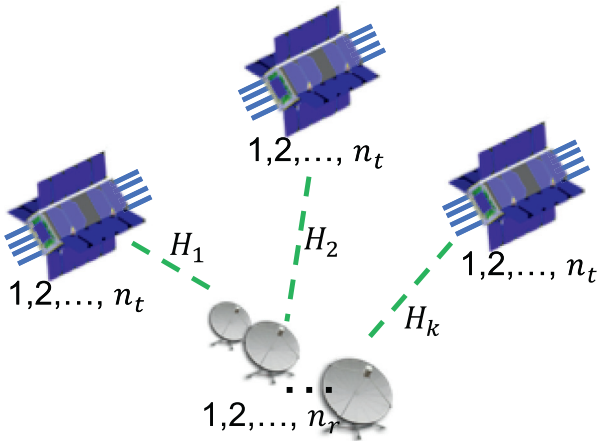

Fig. 9. An illustration of a distributed MIMO communication link in IoST.

As discussed in Section 3.2, the next generation CubeSats will incorporate very large multi-band antenna arrays. Similarly as in the terrestrial case, MIMO [41], massive MIMO [42] and ultra-massive MIMO [35] systems can be utilized. The latter is specially relevant as we move towards mm-wave and THz-band frequencies for satellite communications. The key concept of ultra-massive MIMO communications is to increase the coverage range at mm-wave and THz-band frequencies by simultaneously focusing the transmitted signals in space and in frequency. Ultra-massive MIMO enables different communication modes, ranging from ultra-massive beamforming for maximum communication range; ultra-massive spatial multiplexing, for increased throughput and multi-user capacity; and, multi-band ultra-massive MIMO, which allows simultaneous transmission over multiple mm-wave and THz-band transmission windows. All these modes are enabled by the aforementioned antenna arrays, which can, in addition, be virtually divided in sub-arrays on demand.

4.2.2. Distributed multiple-input multiple-output communication in IoST

Besides MIMO communication across CubeSats, distributed MIMO communication schemes between a set of CubeSats and ground devices, other satellites (e.g., LEO, MEO) or deep-space systems can be created [43]. The advantages of distributed MIMO communication include power and route optimization, as well as higher spatial diversity. With the limited form factor of CubeSats, it is difficult to contain large energy source to boost signal strength, which further limit the capacity of each CubeSat. However, with multiple CubeSats sharing the same task of data transmission, the burden of power consumption is reduced. Moreover, with multiple CubeSats covering the same point of interest, the data routing can be optimally planned. As shown in Fig. 9, three CubeSats, each with n_t antennas, are covering the same ground station with n_r antennas. The distributed MIMO communication is expected to improve the spectral efficiency as well as the energy efficiency of the IoST network.

4.2.3. Resource allocation techniques

To maximize the achievable data-rates in ISLs and GSLs as well as the aggregated network user capacity in the IoST, new resource allocation strategies are needed. In the context of the IoST, the resources available to the CubeSats include: (i) different frequency bands (from RF to THz) with different transmission bandwidths (from 10 MHz to 100 GHz); (ii) different number of antenna elements, which can be virtually grouped in sub-arrays and tuned at the different frequency bands; (iii) different modulation and coding strategies, ranging form the traditional m-PSK and m-QAM with Forward Error Correction (FEC) schemes, to new modulation and coding strategies tailored to the mm-wave and THz-band channels [44]; and, (iv) different medium access control strategies, for unicast, multicast and broadcast information, over the different frequency bands. The resource allocation can be formulated as an optimization problem that can be solved by the help of SDN and machine learning algorithms given the number of devices to be served on Earth, the area on Earth needs to be covered, and the energy provided to each CubeSat [6]. For example, among multiple frequency bands, mm-wave and THz frequencies are desired to serve in the ISL to achieve ultra-fast backbone link. While nowadays on-Earth sensors might not have mm-wave transceivers, the CubeSats can reach ground infrastructure with mm-wave links, as a supplement to lower frequency links. With the proliferation of applications using artificial intelligence and machine learning algorithms, such resource allocation strategies are best optimized with the help of deep learning and clustering algorithms, where the IoST can adaptively select the best available frequency channel, transmit power, modulation and coding scheme, and so on.

4.2.4. Challenges in physical layer techniques

As mentioned before, UM-MIMO communications will enhance the link performance. However, the realization of UM-MIMO schemes in the IoST, however, introduces several challenges. First of all, the performance of UM-MIMO drastically depends on the available channel information. For this, on the one hand, accurate end-to-end channel models accounting for both the impact of the antenna arrays in transmission and reception as well as the propagation medium are needed. While multi-path propagation in the exosphere is highly unlikely, reflections from the CubeSat components (e.g., solar panels) in the vicinity of the receiving antenna need to be taken into account. In addition, as the number of elements in orbit increases and space trash accumulates, reflections and scattering can increase. On the other hand, with the channel models in hand, low-complexity real-time channel estimation and prediction algorithms are needed, which should take into account the relative motion of CubeSats.

In light of the channel information, the second major challenge to address relates to the control and operation of the array. New dynamic beamforming algorithms are needed to implement the different operation modes described above. The control algorithms need to be tailored to the specific array architecture, and in particular, the phase/delay and amplitude control available per element or per group of elements (sub-array). In the simplest case, a predefined codebook with multiple common beam patterns can be designed pre-loaded in the CubeSats, specially taking into account that, once deployed, the CubeSat network topology is not expected to change much. However, in case of CubeSat failure or new

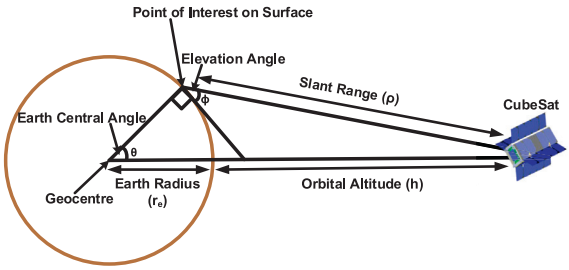

Fig. 10. CubeSat coverage geometry.

additions, the possibility to redefine new codebooks on demand is also desirable.

Additionally, the realization of distributed MIMO systems among CubeSats introduces several open issues. The major roadblock to overcome is the need for accurate time, frequency and phase synchronization between CubeSats. On the one hand, part of this information is already available at the ADCS (see Fig. 1, Section 3). On the other hand, however, this information needs to be accessible and shared among the distributed MIMO CubeSat set, in an efficient manner. Additional challenges include the development of mechanisms to compensate for oscillators deviations in time which can lead to clock skew, phase noise in mm-wave and THz-band transceivers, and changing EM wave propagation speed as it traverses different layers of the atmosphere with different molecules species and concentrations.

5. Constellation design and coverage analysis

Since a single CubeSat has limited footprint coverage of the Earth's surface, a constellation is necessary in order to best serve target areas. Several key parameters are crucial in designing a constellation that can achieve the maximum coverage while minimizing the overall cost of the network. We hereby discuss the number of CubeSats, the number of orbital planes, the elevation angle which determines the coverage of a single CubeSat, the altitude which is a tradeoff between transmission latency and effective coverage area, and the inclination which determines the latitude coverage. In our analysis, we consider that the CubeSats are deployed in a circular orbit in the exosphere, with various possible inclination angles at different altitudes, based on the availabilities of the launch vehicles' orbits [45].

We take a two-step approach towards constellation design. As a first step, we determine the minimum number of CubeSats required for achieving global coverage in GLSs. The numbers thus obtained serves as initial constellation parameters. Then, we determine the number of CubeSats required to achieve a certain maximum separation (in km) required for reliable ISLs, with the values thus obtained representing the final constellation parameters.

5.1. Constellation parameters for global coverage

First, we consider several circular orbits with possible inclination angles including 30°, 60°, and 90° for the study to find the orbital inclination angle with full global coverage. Second, based on Long [46], the minimum number of CubeSats required per orbital plane N_s for complete coverage of a single longitudinal circle is given by,

$$N_s = \lceil 360/(2\theta) \rceil, \tag{1}$$

where θ is the Earth central angle of coverage as shown in Fig. 10, and $\lceil \cdot \rceil$ is the ceiling function. Next, we determine the minimum number of orbital planes for global coverage. In doing so, we recognize that the bulge of the Earth is maximum at the equator. Consequently, if the number of orbital planes in our constellation is sufficient to provide satisfactory coverage at the equator, then this constellation will also prove adequate at every other latitude. A single CubeSat can cover 2θ longitudinal range of the equatorial region, therefore the minimum number of orbital planes N_p required to achieve full coverage of the equatorial region is given by,

$$N_p = \lceil 360/(4\theta) \rceil. \tag{2}$$

The Earth central angle of coverage θ can be obtained by applying the law of sines to the coverage geometry in Fig. 10 as,

$$\sin(\theta) = \frac{\rho}{(h + r_e)} \sin(90 + \phi), \tag{3}$$

where r_e is the Earth's radius, h is the CubeSat's orbital altitude, ρ is the slant range and ϕ is the elevation angle. ρ can be calculated by applying the law of cosines,

$$(r_e + h)^2 = r_e^2 + \rho^2 - 2 r_e \rho \cos(90 + \phi). \tag{4}$$

Using Eq. (1), we plot the minimum number of CubeSats required per orbital plane N_s in Fig. 11(a) by varying the elevation angle ϕ from 5 to 20°, and the orbital altitude h from 500 to 900 km. For example, for an elevation angle of $\phi = 10°$, and an orbital altitude of $h = 500$ km, the number of CubeSats per orbital plane is 16. Fig. 11(a) shows that the CubeSat requirement per orbital plane decreases with increasing altitude and decreasing elevation angle. This is because both an increase in the orbital altitude h, or a decrease in the elevation angle ϕ contribute to an increase in the Earth central angle of coverage θ, and consequently, from Eq. (1), the number of CubeSats required per orbital plane decreases.

Similarly, by using Eq. (2), a plot of the minimum number of orbital planes N_p is obtained in Fig. 11(b), by varying parameters ϕ from 5 to 20°, and h from 500 to 900 km. From Fig. 11(b) it can be observed that a decrease in the elevation angle ϕ or an increase in the altitude h, leads to a decrease in the orbital plane requirement. For example, keeping the elevation angle fixed at $\phi = 10°$, and changing the orbital altitude from $h = 500$ km to $h = 600$ km leads to a decrease in the plane requirement from $N_p = 9$ to $N_p = 8$. This result too can be explained by the fact that parameter θ can be increased by increasing h or decreasing ϕ, and therefore, from Eq. (2), there is a decrease in the number of orbital planes required for global coverage.

In order to further analyze the initial constellation parameters, we consider the inter- and intra-planar distance between the CubeSats. Inter-planar distance is defined as the distance between two adjacent orbital planes, it is maximum at the equator, and decreases towards the poles as the orbits converge. Intra-planar distance refers to the distance between two CubeSats in the same orbital plane. As CubeSats in the same orbital remain stationary relative to each other, their intra-planar separation also remains fixed. These two metrics are of prime importance as they play a vital role in the link budget analysis carried out in Section 4.1. We use the Systems Toolkit (STK) software package to carry out the constellation analysis. Specifically, using STK, we generate Walker-Star constellations for the aforementioned orbital altitudes at a fixed elevation angle of $\phi = 10°$, where every CubeSat is equipped with a sensing device having a field of view $\alpha = 60°$. Fig. 12 shows one such constellation for orbital altitude $h = 800$ km and elevation angle $\phi = 10°$. The distance values are shown in Fig. 13, where we plot the intra-planar distance, and maximum and minimum inter-planar distances for each orbital altitude ranging from $h = 500$ km to $h = 900$ km. For example, for an altitude of $h = 500$ km, the intra-planar separation is given by 2684 km, and maximum and minimum inter-planar separations are 2408 km and 296 km, respectively.

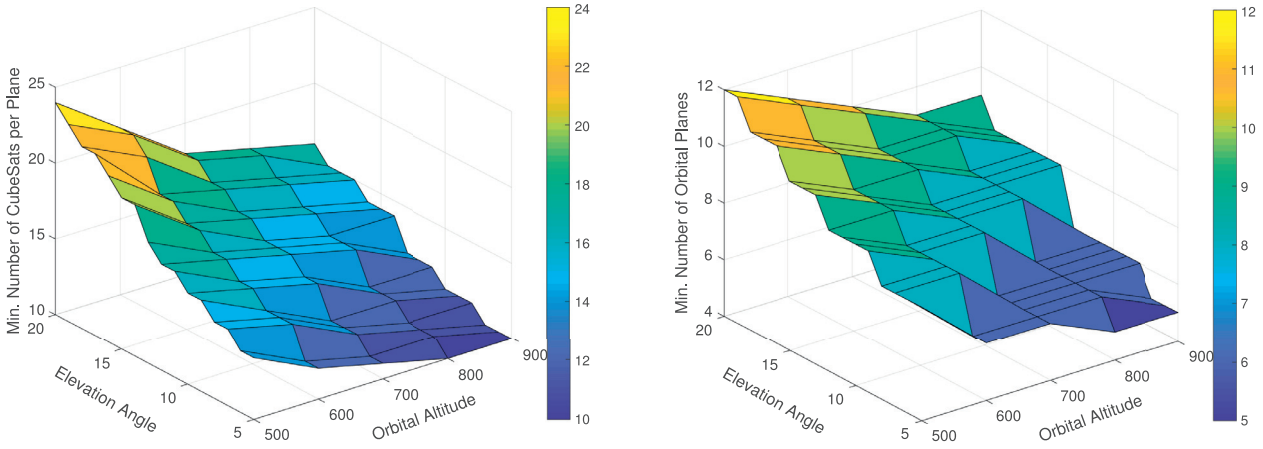

(a) Minimum number of CubeSats per orbital plane. (b) Minimum number of orbital planes.

Fig. 11. Initial constellation parameters.

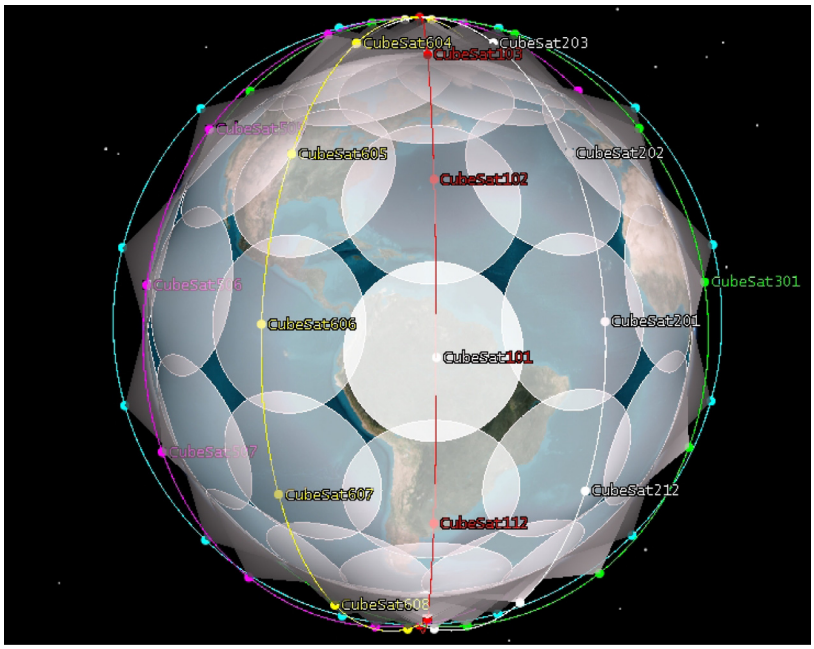

Fig. 12. Walker-Star constellation for global coverage at altitude 800 km and elevation angle 10°.

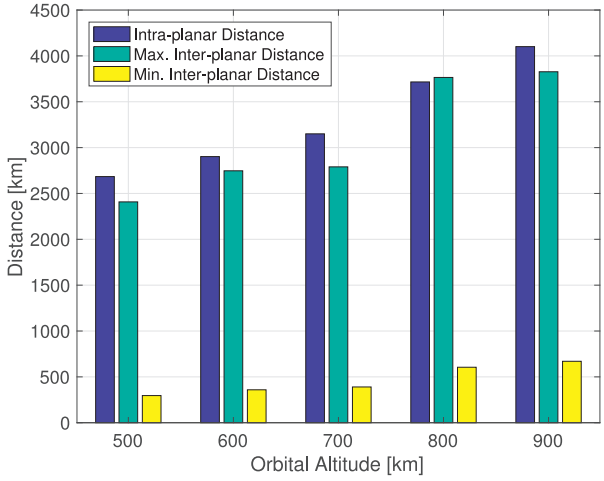

Fig. 13. Intra- and inter-planar separation for initial constellation parameters.

5.2. Constellation parameters for reliable communication

From Fig. 13, we observe that the distances display an increasing trend with increase in orbital altitude. This result can be attributed to the fact that an increase in the orbital altitude causes the circumference of the orbital plane to increase, in addition to increasing the separation between the planes. As a result, the CubeSats grow farther apart as the altitude increases. However, the most important takeaway from Fig. 13 is that even for the lowest altitude of $h = 500$ km the separation between CubeSats is approximately 2500 km, which is too large for reliable communication over high-capacity THz links. Therefore, in order to keep the antenna gain at realizable levels, we scale the number of CubeSats per plane, and the number of orbital planes such that maximum inter- and inter-planar separation is close to 600 km. The parameters of this densified constellation have been shown in Table 2, and serve as the final constellation parameters. From Table 2, we note that the number of CubeSats required per plane has now increased to 71 from 16, and the number of orbital planes has increased to 36 from 9, for $h = 500$ km.

Table 2
Constellation parameters.

Orbital altitude (km)	Orbital inclination (°)	Number of CubeSats per plane	Number of orbital planes
500	30/60/90	71	36
600	30/60/90	72	37
700	30/60/90	73	37
800	30/60/90	74	38
900	30/60/90	75	38

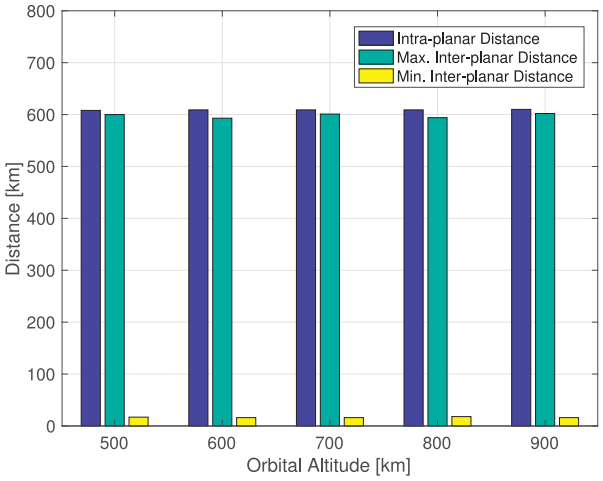

Fig. 14. Intra- and inter-planar separation for final constellation parameters.

Once again, using STK, we obtain the inter- and intra-planar distances for the final constellation parameters as shown in Fig. 14. From Fig. 14, we observe that the maximum separation is now within an acceptable range, with the intra-planar separation for $h = 500$ km being given by 608 km, and 600 km and 17 km being the maximum and minimum inter-planar distances.

5.3. Numerical coverage analysis

Next, we perform coverage analysis of the constellation in terms of key parameters such as (i) percentage of time covered, (ii) average revisit time, and (iii) average access duration, using STK. For the purpose of analysis, we make use of the constellation parameters in Table 2, along with $\phi = 10^\circ$, and $\alpha = 60^\circ$. A point is considered to be in coverage if it lies within the field of view of at least one CubeSat, and the coverage circle of a CubeSat is defined as the instantaneous area of coverage on Earth for that CubeSat. With this, we present the coverage analysis as follows.

5.3.1. Percentage of time covered

The first coverage parameter (or figure of merit) we consider is the percentage of time covered. The percentage of time covered is defined as the average percentage of time for which coverage is present at a given latitude over a 24 h period. Fig. 15(a) shows the percentage of time for which coverage is present for each latitude ranging from -90° to $+90^\circ$, and orbital altitude ranging from $h = 500$ km to $h = 900$ km. From Fig. 15(a), we observe that the figure of merit is fixed at 100% irrespective of the deployment altitude. This result is a direct outcome of the high CubeSat density of the constellation, where every latitude receives coverage from at least one CubeSat at any given point in time. Thus, the constellation is able to achieve continuous global coverage.

5.3.2. Average revisit time

The second figure of merit under consideration is the average revisit time. Revisit time measures the intervals during which coverage is not provided. The average revisit time for a point on the Earth's surface is the average of the durations of all the gaps in coverage over the entire coverage interval of 24 h. Further averaging this metric over all points along a specific latitude provides the average revisit time for that latitude. In Fig. 15(a), we plot this figure of merit for -90° to $+90^\circ$ latitudes, and 500 km to 900 km altitudes. We note that average revisit remains fixed at 0 s for all altitudes, which is an expected outcome in light of the fact that the constellation achieves continuous global coverage as noted in Section 5.3.1, i.e., we do not have any interval of no coverage, and thus the average revisit time is 0 s.

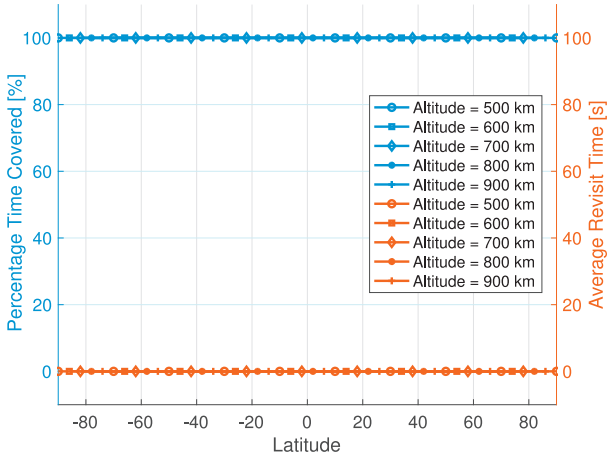

(a) Percentage of time covered and average revisit time.

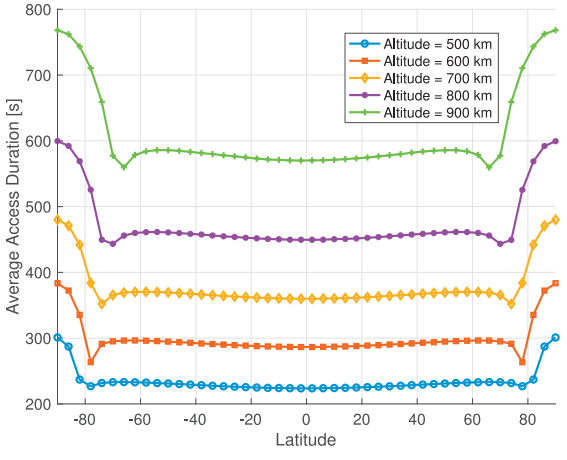

(b) Average access duration.

Fig. 15. Coverage analysis for next-generation CubeSat deployment.

5.3.3. Average access duration

The average access duration is the final figure of merit under consideration. Access duration refers to the time interval during which coverage is present from a single CubeSat. For example, let us consider the Fernbank Observatory in Atlanta, GA as our point of interest. At a given point in time, it is observed that CubeSat 1 covers the observatory for 500 s, followed by a 100-second period of no coverage. This period of no coverage is in turn followed by a coverage duration of 700 s from CubeSat 2. In this case, we have three observation intervals, with an access duration of 500, 0, and 700 s respectively, with the average access duration being given by 600 s, i.e., the average access duration does not take into account periods of no coverage. Averaging over the access duration at each point along a given latitude over a 24-h period leads to the average access duration for that latitude. Fig. 15(b) shows the average access duration for all latitudes, i.e., between -90° and $+90^\circ$, for orbital altitudes ranging from 500 to 900 km.

First, from Fig. 15(b) we observe that the average access duration increases with increase in altitude. This is because the orbital velocity of a CubeSat decreases with increasing orbital altitude, i.e., the farther it is from the Earth, the slower is its orbital velocity. As CubeSats in the higher altitudes move slower, a single CubeSat is able to provide coverage for a longer duration, resulting in a larger access duration. Further, we note that the access duration is maximum at the poles (-90° to -80° and $+80^\circ$ to $+90^\circ$) and decreases towards the equator. Any given point on the Earth in the higher latitudes traverses a shorter distance over a single rotation of the earth, as opposed to a point in the equatorial region. Consequently, the higher latitudes receive coverage from a single CubeSat over a longer duration, resulting in larger access duration values.

To summarize, we note that regardless of the orbital altitude, the next-generation CubeSat constellation achieves continuous global coverage. However, a higher orbital altitude results in larger access duration values which are preferable from a data communications perspective. On the other hand, a higher orbital altitude also requires a larger number of CubeSats as noted in Table 2. Therefore, there exists a design tradeoff that must be adequately addressed based on different applications' needs.

6. Conclusion

This paper presents the design of a new generation of CubeSat, which integrates novel multi-frequency front-ends and antennas able to communicate simultaneously in multiple bands ranging from the microwave to the mm-wave and the THz band. Moreover, through link budget analyses in both intersatellite and ground-satellite links, we show the great capacity potential of such CubeSat communication system. Additionally, a detailed constellation design demonstrates continuous global coverage. The next generation CubeSat is envisioned to serve as a desirable solution for the Internet of Space Things, a paradigm-shift network architecture for future ubiquitous communications.

References

[1] W.A. Hanson, Satellite internet in the mobile age, New Space 4 (3) (2016) 138–152, doi:10.1089/space.2016.0019.

[2] L.A. Davis, L. Filip, How Long Does It Take to Develop and Launch Government Satellite Systems? Technical Report, The Aerospace Corporation, 2015.

[3] R.P. Welle, The CubeSat Paradigm: An Evolutionary Approach to Satellite Design, Technical Report, The Aerospace Corporation, 2016.

[4] J. Puig-Suari, C. Turner, W. Ahlgren, Development of the standard CubeSat deployer and a CubeSat class picosatellite, in: Proceedings of the IEEE Aerospace Conference, 1, 2001, pp. 1/347–1/353, doi:10.1109/AERO.2001.931726.

[5] K. Woellert, P. Ehrenfreund, A.J. Ricco, H. Hertzfeld, CubeSats: cost-effective science and technology platforms for emerging and developing nations, Adv. Space Res. 47 (4) (2011) 663–684.

[6] I.F. Akyildiz, A. Kak, The Internet of Space Things, In press, 2018.

[7] O.P. Gupta, Iridium NEXT Sensor PODs: global access for your scientific payloads, in: Proceedings of the 25th Annual AIAA/USU Conference on Small Satellites, 2011.

[8] M. Baylor, Planet labs targets a search engine of the world, 2018, (https://www.nasaspaceflight.com/2018/01/planet-labs-targets-search-engine-world/).

[9] Jet Propulsion Laboratory and NASA, NASA's first image of Mars from a CubeSat, 2018, (https://www.jpl.nasa.gov/news/news.php?feature=7263).

[10] J. Foust, ELSE raises $3 million for Internet of Things nanosatellite constellation, 2017, (https://spacenews.com/else-raises-3-million-for-internet-of-things-nanosatellite-constellation/).

[11] C. Henry, Fleet details 100 nanosat constellation for Internet of Things connectivity, 2017, (https://spacenews.com/fleet-details-100-nanosat-constellation-for-internet-of-things-connectivity/).

[12] Kepler Communications, Kepler Receives FCC Approval to Access US Market for Satellite Communication Services, 2018, (https://www.keplercommunications.com/newsroom/press-releases/post/kepler-receives-fcc-approval-to-access-us-market-for-satellite-communication-services).

[13] K. Russell, Aerial & Maritime, Aistech Enter Mutual Data Service Agreement, 2017, (https://www.satellitetoday.com/telecom/2017/03/31/aerial-maritime-aistech-enter-mutual-data-service-agreement/).

[14] S. Madry, Space Systems for Disaster Warning, Response, and Recovery (SpringerBriefs in Space Development), Springer, 2014.

[15] R. Hevner, W. Holemans, J. Puig-Suari, R. Twiggs, An advanced standard for CubeSats, in: Proc. of the 25th Annual AIAA/USU Conference on Smallsats, 2011, 2011 https://digitalcommons.usu.edu/smallsat/2011/all2011/15/.

[16] N. Crisp, K. Smith, P. Hollingsworth, Launch and deployment of distributed small satellite systems, Acta Astronaut. 114 (2015) 65–78, doi:10.1016/j.actaastro.2015.04.015.

[17] T.C. Program, Poly Picosatellite Orbital Deployer Mk. III Rev. E User Guide, Technical Report, 2014.

[18] L.J. Ippolito, L.J. Ippolito Jr, Satellite Communications Systems Engineering: Atmospheric Effects, Satellite Link Design and System Performance, John Wiley & Sons, 2017.

[19] J. Straub, M. Wegerson, R. Marsh, An intelligent attitude determination and control system for a CubeSat class spacecraft, in: Proceedings of the AIAA SPACE Conference and Exposition, 2015, p. 4422.

[20] Z. Pi, F. Khan, An introduction to millimeter-wave mobile broadband systems, IEEE Commun. Mag. 49 (6) (2011) 101–107, doi:10.1109/mcom.2011.5783993.

[21] I.F. Akyildiz, J.M. Jornet, C. Han, Terahertz band: next frontier for wireless communications, Phys. Commun. 12 (2014) 16–32.

[22] V.W. Chan, Optical satellite networks, J. Lightwave Technol. 21 (11) (2003) 2811.

[23] Z. Sodnik, B. Furch, H. Lutz, Optical intersatellite communication, IEEE J. Sel. Top. Quant. Electron. 16 (5) (2010) 1051–1057.

[24] A.H.M. Shirazi, A. Nikpaik, R. Molavi, S. Lightbody, H. Djahanshahi, M. Taghivand, S. Mirabbasi, S. Shekhar, On the design of mm-wave self-mixing-VCO architecture for high tuning-range and low phase noise, IEEE J. Solid State Circuits 51 (5) (2016) 1210–1222.

[25] J.M. Jornet, I.F. Akyildiz, Graphene-based plasmonic nano-transceiver for Terahertz band communication, in: Proceedings of the 8th European Conference on Antennas and Propagation (EuCAP 2014), IEEE, 2014, pp. 492–496. US Patent: 9397758 B2 doi: 10.1109/EuCAP.2014.6901799.

[26] I. Mehdi, J.V. Siles, C. Lee, E. Schlecht, THz diode technology: status, prospects, and applications, Proc. IEEE 105 (6) (2017) 990–1007.

[27] T.W. Crowe, W.R. Deal, M. Schröter, C.-K. C. Tzuang, K. Wu, Terahertz RF electronics and system integration, Proc. IEEE 105 (6) (2017) 985–989.

[28] A. Rashidinejad, Y. Li, A.M. Weiner, Recent advances in programmable photonic-assisted ultrabroadband radio-frequency arbitrary waveform generation, IEEE J. Quant. Electron. 52 (1) (2016) 1–17, doi:10.1109/JQE.2015.2506987.

[29] J. Wang, H. Shen, L. Fan, R. Wu, B. Niu, L.T. Varghese, Y. Xuan, D.E. Leaird, X. Wang, F. Gan, et al., Reconfigurable radio-frequency arbitrary waveforms synthesized in a silicon photonic chip, Nat. Commun. 6 (2015) 5957.

[30] P. Ghelfi, G. Serafino, F. Scotti, F. Laghezza, A. Bogoni, Flexible receiver for multiband orthogonal frequency division multiplexing signals at the millimeter waveband based on optical downconversion, Opt. Lett. 37 (18) (2012) 3924–3926.

[31] F. Laghezza, F. Scotti, P. Ghelfi, A. Bogoni, Photonics-assisted multiband RF transceiver for wireless communications, J. Lightwave Technol. 32 (16) (2014) 2896–2904.

[32] X. Yang, K. Xu, J. Yin, Y. Dai, F. Yin, J. Li, H. Lu, T. Liu, Y. Ji, Optical frequency comb based multi-band microwave frequency conversion for satellite applications, Opt. Expr. 22 (1) (2014) 869–877.

[33] C.G. Christodoulou, Y. Tawk, S.A. Lane, S.R. Erwin, Reconfigurable antennas for wireless and space applications, Proc. IEEE 100 (7) (2012) 2250–2261.

[34] X. Liu, S. Yao, B.S. Cook, M.M. Tentzeris, S.V. Georgakopoulos, An origami reconfigurable axial-mode bifilar helical antenna, IEEE Trans. Antennas Propagat. 63 (12) (2015) 5897–5903.

[35] I.F. Akyildiz, J.M. Jornet, Realizing ultra-massive MIMO (1024 × 1024) communication in the (0.06–10) terahertz band, Nano Commun. Netw. 8 (2016) 46–54.

[36] L. Zakrajsek, E. Einarsson, N. Thawdar, M. Medley, J.M. Jornet, Design of graphene-based plasmonic nano-antenna arrays in the presence of mutual coupling, in: Proceedings of the 11th European Conference on Antennas and Propagation (EuCAP), 2017.

[37] S.V. Hum, J. Perruisseau-Carrier, Reconfigurable reflectarrays and array lenses for dynamic antenna beam control: a review, IEEE Trans. Antennas Propag. 62 (1) (2014) 183–198.
[38] J.V. Siles, K.B. Cooper, C. Lee, R. Lin, G. Chattopadhyay, I. Mehdi, A new generation of room-temperature frequency multiplied sources with up to 10x higher output power in the 160 ghz-1.6 thz range, IEEE Trans. Terahertz Sci. Technol. (2018), doi:10.1109/TTHZ.2018.2876620.
[39] S.K. Saha, Y. Ghasempour, M.K. Haider, T. Siddiqui, P. De Melo, N. Somanchi, L. Zakrajsek, A. Singh, R. Shyamsunder, O. Torres, et al., X60: a programmable testbed for wideband 60 ghz wlans with phased arrays, Comput. Commun. 133 (2019) 77–88.
[40] J.Y. Suen, M.T. Fang, P.M. Lubin, Global distribution of water vapor and cloud cover – sites for high-performance THz applications, IEEE Trans. Terahertz Sci. Technol. 4 (1) (2014) 86–100, doi:10.1109/TTHZ.2013.2294018.
[41] P.-D. Arapoglou, K. Liolis, M. Bertinelli, A. Panagopoulos, P. Cottis, R. De Gaudenzi, MIMO over satellite: a review, IEEE Commun. Surv. Tutor. 13 (1) (2011) 27–51.
[42] R.C. de Lamare, Massive MIMO systems: signal processing challenges and future trends, URSI Radio Sci. Bull. 86 (4) (2013) 8–20.
[43] R.J. Barton, Distributed MIMO communication using small satellite constellations, in: Proceedings of the IEEE International Conference on Wireless for Space and Extreme Environments (WiSEE), 2014, pp. 1–7, doi:10.1109/WiSEE.2014.6973070.
[44] C. Han, I.F. Akyildiz, Distance-aware bandwidth-adaptive resource allocation for wireless systems in the terahertz band, IEEE Trans. Terahertz Sci. Technol. 6 (4) (2016) 541–553.
[45] A. Marinan, A. Nicholas, K. Cahoy, Ad hoc CubeSat constellations: secondary launch coverage and distribution, in: Proceedings of the IEEE Aerospace Conference, 2013, pp. 1–15, doi:10.1109/AERO.2013.6497174.
[46] F. Long, Satellite Network Robust QoS-aware Routing, Springer, 2014.

Ian F. Akyildiz is currently the Ken Byers Chair Professor in Telecommunications with the School of Electrical and Computer Engineering, Director of the Broadband Wireless Networking Laboratory, and Chair of the Telecommunication Group at Georgia Institute of Technology, Atlanta, USA. Since 2011, he serves as a Consulting Chair Professor with the Department of Information Technology, King Abdulaziz University, Jeddah, Saudi Arabia, and with the Computer Engineering Department at the University of Cyprus since January 2017. He is a Megagrant Research Leader with the Institute for Information Transmission Problems at the Russian Academy of Sciences, in Moscow, Russia, since May 2018. His current research interests are in 5G wireless systems, nanonetworks, Terahertz band communications, and wireless sensor networks in challenged environments. He is an IEEE Fellow (1996) and an ACM Fellow (1997). He received numerous awards from the IEEE and the ACM, and many other organizations. His h-index is 115, and the total number of citations is above 105 K as per Google scholar as of November 2018.

Josep M. Jornet received the B.S. degree in telecommunication engineering and the M.Sc. degree in information and communication technologies from the Universitat Politècnica de Catalunya, Barcelona, Spain, in 2008, and the Ph.D. degree in electrical and computer engineering from the Georgia Institute of Technology (Georgia Tech), Atlanta, GA, USA, in 2013. From 2007 to 2008, he was a Visiting Researcher with the Massachusetts Institute of Technology (MIT), Cambridge, under the MIT Sea Grant Program. He is currently an Assistant Professor with the Department of Electrical Engineering, University at Buffalo, The State University of New York. He was the recipient of the Oscar P. Cleaver Award for outstanding graduate students in the School of Electrical and Computer Engineering, at Georgia Tech in 2009. He also received the Broadband Wireless Networking Lab Researcher of the Year Award in 2010. In 2016, 2017 and 2018, he received the Distinguished TPC Member Award at the IEEE International Conference on Computer Communications (INFOCOM). In 2017, he received the IEEE Communications Society Young Professional Best Innovation Award, the ACM NanoCom Outstanding Milestone Award and the UB SEAS Early Career Researcher of the Year Award. His current research interests are in Terahertz-band communication networks, Nanophotonic wireless communication, Intra-body Wireless Nanosensor Networks and the Internet of Nano-Things. In these areas, he has co-authored more than 100 peer-reviewed scientific publications, 1 book, and has also been granted 3 US patents. Since July 2016, he is the Editor-in-Chief of the Nano Communication Networks (Elsevier) Journal and serves in the Steering Committee of the ACM/IEEE NanoCom Conference Series. He is a member of the IEEE, the ACM and the SPIE

Shuai Nie received the B.S. degree in Telecommunications Engineering from Xidian University in 2012, and the M.S. degree in Electrical Engineering from New York University in 2014. Currently, she is working toward the Ph.D. degree in electrical and computer engineering at the Georgia Institute of Technology under the supervision of Prof. Ian F. Akyildiz. Her research interests include terahertz band and millimeter-wave communication networks and the wireless communication system for 5G and beyond.